Wood Sci Technol (2014) 48:591–609
DOI 10.1007/s00226-014-0626-3

ORIGINAL

Water vapour diffusion through historically relevant glutin-based wood adhesives with sorption measurements and neutron radiography

D. Mannes · S. Sanabria · M. Funk · R. Wimmer · K. Kranitz · P. Niemz

Received: 11 October 2013 / Published online: 22 March 2014

Abstract In this work, the sorption and moisture diffusion behaviour of historically relevant glutin-based adhesives (i.e. bone glue, hide glue, fish glue) is characterized. The adhesive's sorption isotherms were assessed on thin film samples revealing fundamental differences between the glutin-based adhesives and the synthetic reference adhesive (polyurethane). Furthermore, the water vapour diffusion parallel to the fibre was examined by means of neutron imaging on bonded two-layer samples of Norway spruce wood. In contrast to previous studies using neutron imaging, a new evaluation approach is presented, which allows for nonzero initial moisture conditions and takes into account and compensates for the geometry changes in the sample caused by swelling and shrinkage, thus allowing for a characterization of the diffusion behaviour within the glue line. The diffusion coefficients determined with neutron imaging were interpreted in terms of a theoretical model which takes into account the glue line microstructure. Although the diffusion coefficients were on average larger values for the glutin-based adhesives compared to the reference polyurethane adhesive, the significant variation observed in the sorption measurement is not reflected. This can partially be ascribed to excessive penetration of the adhesives into the wood substrate in fibre direction, which impedes a continuous adhesive layer. Furthermore, deformation and densification of the wood structure was assessed in the vicinity of the adhesive joint. This

D. Mannes (✉)
Neutron Imaging and Activation Group, Paul Scherrer Institut, Villigen, Switzerland
e-mail: david.mannes@psi.ch

S. Sanabria · K. Kranitz · P. Niemz
Institut für Baustoffe, Gruppe Holzphysik, ETH Zürich, Zürich, Switzerland

M. Funk
Abteilung Holztechnologie und Holzwerkstoffe, Universität Göttingen, Göttingen, Germany

R. Wimmer
Institut für Naturstofftechnik, IFA Tulln, Universität für Bodenkultur Wien, Vienna, Austria

effect can be ascribed to the surface roughness, which results in very high local stresses leading to buckling and deformation of the tracheids. This situation is similar to that found for adhesive joints in or close to the fibre direction such as finger or butt joints.

Introduction

Fluctuations of the ambient climate can induce cracks or delamination in glued wooden cultural heritage objects such as antique musical instruments or furniture. There is increasing interest from museums and conservators in investigations directed towards the understanding and minimization of these failure processes. In particular, the development of models simulating climate-induced stress states requires knowledge of the sorption and diffusion behaviour of the gluing products. Most adhesives which are traditionally used for furniture making, veneering or instrument making are glutin based (e.g. fish glue, hide glue, bone glue). Their properties differ substantially from modern synthetic adhesives, and data are hardly available. In this context, this work as part of the COST action IE-0601 "Wood Science for Conservation of Cultural Heritage (WoodCultHer)" aimed at the development and application of methodologies for the characterization of sorption and moisture diffusion behaviour of historically relevant adhesives.

In general, the diffusion behaviour of glued wood samples is tested in sorption experiments according to DIN ISO 12572 (2001) in dry cup/wet cup experiments. The result of such an experiment expresses a mean value valid for the whole specimen, i.e. wood lamellas together with adhesive layer. Glutin-based adhesives are known to absorb more moisture than other adhesives and they also have higher diffusion coefficients (Volkmer et al. 2012). While these characteristics are relevant for the conservation and safekeeping of cultural heritage objects, they are scientifically not well documented and described.

For the modelling of moisture transport and delamination, spatially resolved information is required. One method to assess the moisture transport is neutron radiography which allows quantifying and localizing moisture within the wood specimen (Mannes et al. 2009a). Sonderegger et al. (2010) investigated the diffusion behaviour of wood bonded with different synthetic adhesives perpendicular to the fibre direction. A difference between the moisture-dependent diffusion coefficients of the adhesives was determined. However, this methodical approach suffers from several limitations. Due to the low rate of diffusion and transport through the cell walls, the experiments had to be conducted over several months, which is unpractical due to the constrained beam times at the neutron imaging facility. The diffusion coefficient optimization procedure requires initially oven-dried samples for reference imaging. The drying procedure might in turn lead to (although small) thermal modification effects of the wood microstructure, with the consequence of influencing the sorption behaviour (Kollmann 1965). Moreover, during preparation and handling, the samples resorb water (3–5 %) in a way the required dry reference state is in fact not achieved. Finally, moisture-induced swelling deformation during the neutron measurement leads to misalignment of the samples imaged at different

states. As a consequence, the calculated moisture maps show strong artefacts and discontinuities (glue lines outer edges). Moreover, the local moisture concentration is a function of both neutron transmission and swelling strain. Neglecting the latter in the computation leads to quantitative uncertainties in the calculated moisture values. Therefore, for an accurate quantification and localization of moisture, the deformation fields need to be calculated. Lanvermann et al. (2013) addressed this problem by combining neutron imaging with an optical image correlation system (VIC 3D). The latter consists of two CCD cameras, which continuously record a speckle pattern sprayed onto the sample. The acquired data are used to calculate the sample surface deformation fields with high spatial resolution. Although spatially accurate, this set-up is intricate, and it is mainly used for the investigation of the influence of the heterogeneous wood microstructure on the moisture transport. For diffusion analysis across adhesive bonding, the wood substrates are generally approximated to homogeneous layers. A simple deformation correction based exclusively on neutron radiographies is in this case desirable.

In this work, the sorption and moisture diffusion behaviour of historically relevant glutin-based adhesives was investigated by the following hypotheses: (1) fundamental differences between glutin-based adhesives and a reference synthetic adhesive can be assessed through sorption isotherms. For wood glue line characterization, the above stated methodological limitations for neutron imaging can be overcome without additional equipment as follows: (2) nonzero initial moisture conditions and sample deformation can be accounted for by exclusively improving the data evaluation of the neutron radiographies, and (3) an alternative sample preparation method which is discussed later, can significantly reduce measurement time.

The stated hypotheses are tested. Potential and applicability of the modified neutron imaging method are discussed.

Materials and methods

Adhesive samples

In this investigation, four different adhesives were investigated. Three of them were glutin-based, and they are fish glue, hide glue and bone glue (Kremer Pigmente, Aichstetten, Germany). As synthetic reference, the one-component polyurethane resin (1C-PUR) (Purbond AG, Sempach Station, Switzerland) was chosen. Table 1 provides specific values for the adhesives used according to manufacturer's data sheets.

Specimens for the neutron measurements consisted of two-layered samples of Norway spruce (*Picea abies (L.) Karst.*), which were glued together in radial-tangential (RT) plane. The overall dimensions of the samples were $10 \times 30 \times 40$ mm^3 in the radial (R), tangential (T) and longitudinal direction (L). From each adhesive type, four samples were produced and tested. Standard screw clamps were applied to join the parts. The exact pressure applied over the glue line during curing could hence not be determined. The gluing in the RT plane

Table 1 Characteristics of the investigated adhesives (based on manufacturers data sheets)

Adhesive	1 C-PUR	Fish glue	Hide glue	Bone glue
Manufacturer/type	Purbond HB S309	Fish glue 63550, Kremer Pigmente	Hide glue cubes 63010, Kremer Pigmente	Bone glue pearls 63000, Kremer Pigmente
Viscosity (mPa s)	24,000	4,000	60–120	40–80
Application rate (ml m^2) [* (g m^2)]	120–160*	60–**150**–200	70–**150**–200	70–**150**–200
pH	–	4–6	5.5–7.5	5.5–7.5
Solids content (%)	100	Approximately 45	2–50 (in solution)	2–50 (in solution)
Solubility in water	Insoluble	Soluble	Soluble	Soluble
Form of delivery	Liquid	Liquid	Cubes	Pearls
Density (at 20 °C) (g cm^3)	1.16	1.17	Approximately 1.10	1.20

constrains the moisture transport parallel to the fibre direction, which allowed 14…19 times faster diffusion than in the cross-fibre plane (Sonderegger et al. 2010) reducing the measurement time to about 12 h.

Prior to the actual neutron imaging measurements, the specimens were conditioned at 20 °C and 35 %RH, resulting in an initial wood moisture of approximately $u_o = 8$ % at the beginning of the experiment. The initial moisture content was chosen to represent the praxis-relevant moisture values of wooden cultural heritage objects in dry environments (Gereke et al. 2011).

Sorption isotherms of adhesive films

For the sorption measurements, adhesive films were produced through fill spreading of the liquid adhesives onto a plastic film and smoothing of the surface with a film applicator frame. The ambient climate was individually adjusted to meet the proper reactivity and curing characteristics. After curing, the final film thickness was 0.15 mm throughout. Sorption isotherms of the cured adhesive films were determined using a DVS Advantage® apparatus (DVS, Surface Measurement Systems Ltd, London, UK). This equipment allowed the determination of sorption isotherms at constant temperature using a range of preset relative humidity (RH). The apparatus holds two measurement pans, a sample and reference pan, suspended by arms of a SMS UltraBalance™ microbalance (sensitivity 0.1 µg). Sample and reference holders were connected to the microbalance by hanging wires on two arms in a chamber, both being thermostatically controlled. With a constant flow of nitrogen gas in the system, a preset amount of water vapour was mixed and did pass through the chamber to maintain the set relative humidity level. Runs started at 0 %RH and increased in 5 and 10 % steps up to a maximum of 98 %RH, before descending to zero relative humidity. Humidity and temperature probes were located in the vicinity of the sample and reference holders providing accurate data. Adhesive films were pre-dried prior to measurement. Pre-drying of the films was

continued at 0 %RH in the chamber and as soon as stability was reached. All water sorption experiments were carried out in the chamber at a temperature of 25 °C.

Determination of the wood moisture by means of neutron imaging

Experimental set-up

The experiments were performed at the neutron imaging facility NEUTRA (Lehmann et al. 2001) situated at the Swiss spallation neutron source SINQ, Paul Scherrer Institute, Villigen, Switzerland (Blau et al. 2009). The detector used for the experiments consisted of a scintillator–CCD-camera-system with 1,024 × 1,024 pixels, a 100-µm-thick ^{6}LiF/ZnS scintillator and a field of view of approximately 15 cm, resulting in a pixel size of 148 µm/pixel. The exposure time for single images was 5 s.

The experiments were carried out analogous to the experiments described in Mannes et al. (2009a). The water vapour diffusion occurred in glued two-layered wood specimens exposed to different climates (high relative humidity (RH) on one side, low RH on the other side). After conditioning at 20 °C/35 %RH, the samples were insulated with aluminium tape on four sides, thus defining the diffusion direction along the fibre and through the adhesive joint (Fig. 1). The insulated samples were subsequently fixed onto a box filled with silica gel. This assembly was placed in a neutron transparent box with moist climate (29–30 °C and 90 %RH) for the duration of the experiment. The relative humidity below the samples accounted for approximately 3–5 %RH above the silica gel.

Data evaluation

The basic principles of quantitative neutron imaging of wood are described in Mannes (2009) and Mannes et al. (2009b), whereas the principles of the

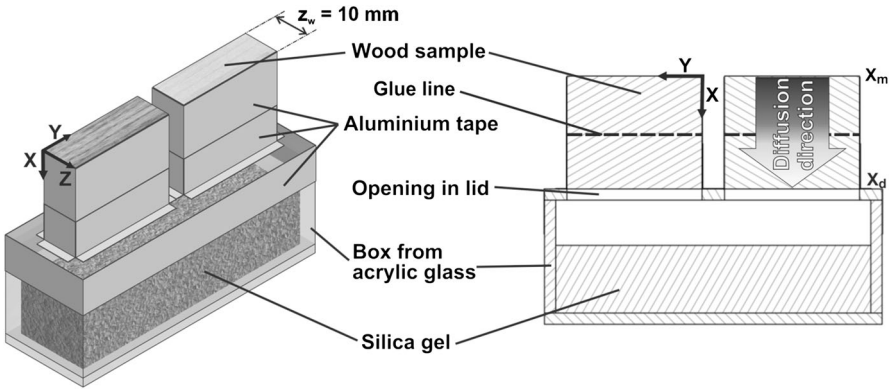

Fig. 1 Experimental set-up for neutron imaging together with coordinate axis definition; the neutron beam travels parallel to the *Z axis*, the moisture diffusion occurs along the X direction from the moist surface (Xm) to the dry surface (Xd) (modified from Mannes et al. 2009a)

determination of moisture content maps from neutron images are given in Mannes et al. (2009a), (2012) and Sonderegger et al. (2010). Here, only the modifications to include sample deformation and nonzero initial moisture content are described.

Just like X-radiography, neutron radiography is based on the principle of transmission measurements, with the transmission coefficient T following in a first order approximation Lamberts-Beer law:

$$-\ln T = -\ln I/I_0 = \Sigma_{\text{eff}} z = -\left(\frac{\Sigma}{\rho}\right)_{\text{w}} \cdot \rho_{\text{w}}/Q \cdot z_{\text{w}} + \left(\frac{\Sigma}{\rho}\right)_{\text{h}} \cdot \rho_{\text{h}} \cdot z_{\text{h}} \tag{1}$$

where T is the transmission, I is the intensity of the transmitted radiation, I_0 the intensity of the incident radiation, Σ_{eff} the effective attenuation coefficient and z the thickness of the sample in beam direction. Σ_{eff} is a mixture of dry wood and moisture components. Equation 1 is here modified with respect to Mannes et al. (2009a) to include the in-plane swelling $Q = (1 + \varepsilon_{\text{xx}})(1 + \varepsilon_{\text{yy}})$ of the radiography pixel with respect to the reference dry state (ε_{ii} are strain components). Q is estimated by calculating the deformation of individual wood lamellas for each recorded moisture state, as described below. $(\Sigma/\rho)_w = 0.18\ \text{m}^2\ \text{kg}^{-1}$ and $(\Sigma/\rho)_h = 0.35\ \text{m}^2\ \text{kg}^{-1}$ are mass-attenuation coefficients experimentally determined at NEUTRA. The values refer to the densities in dry wood ρw and water ρh, respectively (Hassanein 2006; Mannes et al. 2009b); z represents the effective attenuation lengths through dry wood (index w) and water (index h). ρ_{w} and ρ_{h} are constant values during the experiment. The effective wood substance density ρ_{w}/Q is reduced as the sample swells (Eq. 1). The out-of-plane swelling $(1 + \varepsilon_{\text{zz}})$ leads simultaneously to an increase in the effective attenuation length and a decrease in the effective wood substance density, which cancel in Eq. 1.

The local moisture content $u(t)$ at time t is defined with respect to the masses of deformed $m_{\text{u}}(t)$ [transmission coefficient $T(t)$] and undeformed m_{d} (ideal dry state—not available) pixels:

$$u(t) = \frac{m_u(t) - m_d}{m_d} = Q\frac{\rho_{\text{h}} z_{\text{h}}}{\rho_{\text{w}} z_{\text{w}}} \tag{2}$$

However, by referring to the initial homogeneous moist state u_o (transmission coefficient T_{o}), it is possible to quantify moisture changes at arbitrary points in the images. Applying Eqs. 1 and 2 leads to:

$$u(t) = \frac{(\Sigma/\rho)_{\text{w}}}{(\Sigma/\rho)_{\text{h}}}\left[\frac{\ln T(t)}{\ln T_0}\frac{Q(t)}{Q_0} - 1\right] + \left[\frac{\ln T(t)}{\ln T_0}\frac{Q(t)}{Q_0}u_0\right] \tag{3}$$

Equation 3 only requires knowledge of the surface change $Q(t)/Q_o$ of the pixels between test and initial state.

Previous to $u(t)$ calculation with Eq. 3, an additional image processing step was implemented in *Matlab*® to compensate sample deformation and align the neutron images $T(t)$ and T_o. In a first step, the four sides of the sample and the glue line are automatically determined within the images. Every lamella is described as a tetragon, which is defined by the four straight lines R_{r}, R_{t}, R_{b}, and R_{l} (Fig. 2a). For the deformation correction, an equidistant grid is fitted to the edges of the lamella

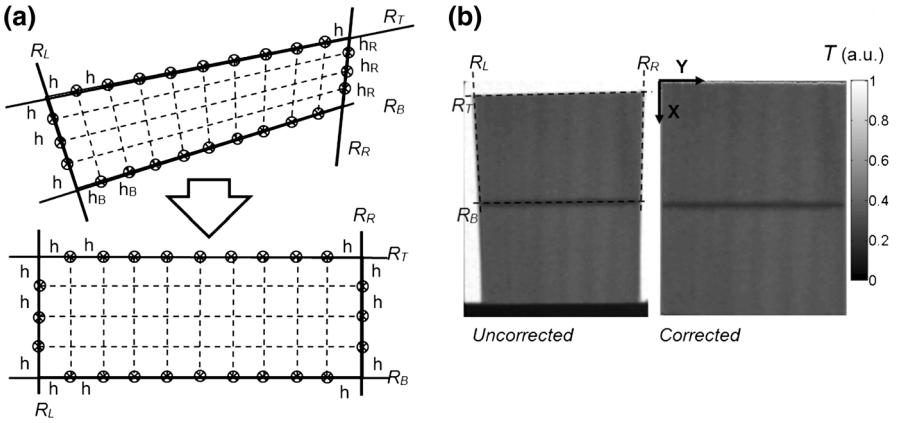

Fig. 2 Deformation correction in neutron images. **a** Image referencing method. **b** Neutron transmission images before (uncorrected) and after (corrected) deformation correction

(respectively to the defining lines). Subsequently, the thus defined image section is transformed in order to obtain a non-deformed rectangle with adapted scale (Fig. 2b). For each pixel, the surface ratio between pixel areas in $T(t)$ and T_o gives $Q(t)/Q_o$.

After deformation and scattering corrections, the wood moisture content can be calculated with Eq. 3. The moisture distribution is visualized as a function of time (Fig. 3).

The calculation of the diffusion coefficients is an extension of the nonlinear optimization method described in Sonderegger et al. (2010) for nonzero initial moisture content u_o. The unsteady-state bound water diffusion is approximated with Fick's second law:

$$\begin{array}{ll} \partial_t u = \partial_x (D \partial_x u) & D = D_o \exp(\alpha u) \\ -D\partial_x u = \sigma_m \left[u(x,t) - u_{\infty,m}\right] & (x,t) \in \Gamma[m,t] \\ -D\partial_x u = \sigma_d \left[u(x,t) - u_{\infty,d}\right] & (x,t) \in \Gamma[d,t] \\ u(x,t) = u_o & (x,t) \in \Gamma[x,0] \end{array} \quad (4)$$

where D is the moisture-dependent diffusion coefficient parameterized as a function of the coefficients D_o and α. σ are surface emission coefficients describing the influence of external resistance on moisture movement and u_∞ the equilibrium moisture content at the boundaries, which due to the nonzero initial u_o are optimized for both the moist m and dry d boundaries of X. This yields a total of eight optimization parameters $D_{o,j}$, $D_{o,w}$, α_j, α_w, (diffusion in wood and glue joint region, respectively) $u_{\infty,m}$, $u_{\infty,d}$, σ_m and σ_d, with respect to the six parameters of the problem for zero u_o. In order to achieve a well-conditioned optimization problem with the increased number of fit parameters, the magnitudes of σ_m and σ_d were assumed of equal magnitude and of opposite sign. This simplification neglects moisture dependencies of σ, which, in general and particularly for the observed small moisture variation range (6…12 %, Fig. 3), are not expected to be large (Eitelberger and Svensson 2012). The start values for $u_{\infty,m}$ and $u_{\infty,d}$ are extracted

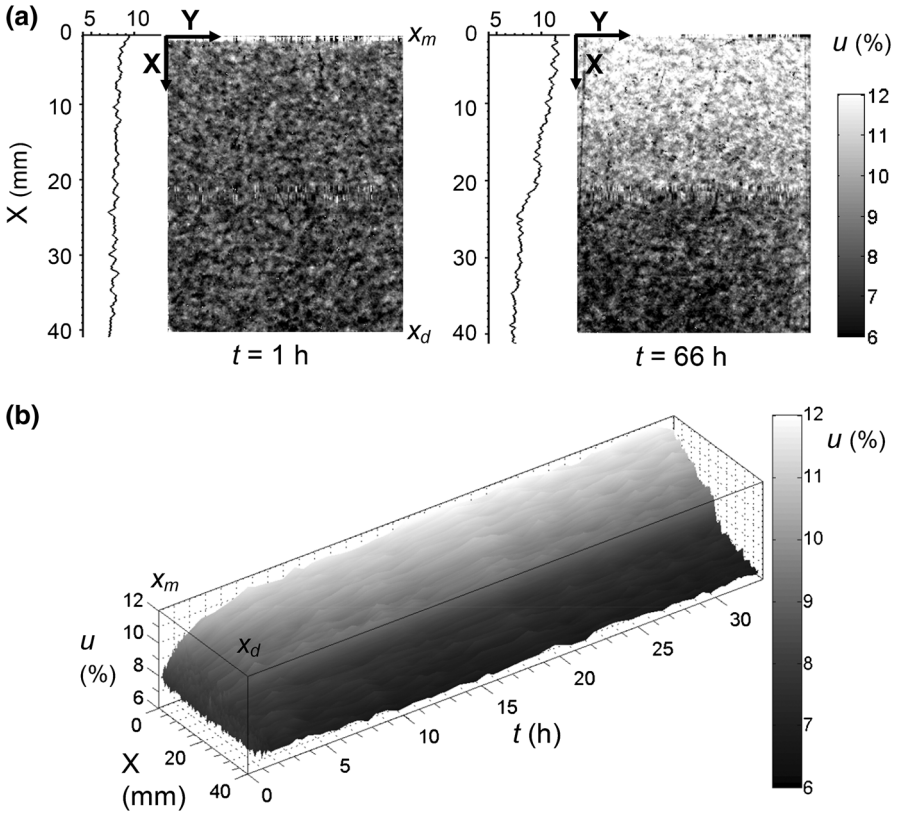

Fig. 3 Wood moisture content determined by neutron imaging versus time. **a** Time snapshots of moisture content distribution u over a sample bonded with fish glue at the beginning of the diffusion experiment (t = 1 h) and in steady state (t = 66 h); **b** mean moisture profile along the diffusion direction (X) as a function of time

from the moisture content at sample boundaries at latest instants of time. A consistent convergence for all samples is ensured with a four-step optimization for which the number of optimization parameters was successively increased: I) D_j, σ_m, II) D_j, σ_m, D_w, III) D_j, σ_m, D_w, u_d, u_m, IV) D_j, σ_m, D_w, u_d, u_m, α_a, α_w. The optimization is based on a "Nelder-Mead simplex direct search" with respect to an error function $e_u = \sqrt{\frac{1}{N_t}\frac{1}{N_x}\sum_t \sum_x \left[u_{\mathrm{sim}}(x,t) - u_{\mathrm{meas}}(x,t)\right]^2}$ between measured u_{meas} (neutron radiography) and simulated u_{sim} (Eq. 4) moisture contents. The random noise level is reduced by calculating e_u with respect to time-averaged u_{meas} and u_{sim} profiles.

Modelling of macroscopic moisture diffusion through bond line microstructure

The influence of the cellular microstructure on the macroscopic moisture diffusion along softwood timbers glued in fibre direction was analysed in order to relate the diffusion coefficient D_{j} evaluated in "Data evaluation" to the diffusion properties of

the adhesive D_a. The glue joint region was described in terms of a pure adhesive phase of thickness ξ_a, and an interphase consisting of tracheid cells with lumina filled with adhesive (Fig. 4a). For simplification, wood cells of constant dimensions are modelled with lumen diameter and the lateral cell wall width t_{RT}. Moreover, it is assumed that the position of the cell boundary along the fibre direction (thickness t_L) follows a uniform random distribution and that lumina interfacing the glue line are completely adhesive filled. The fraction of adhesive-filled voids f_a then linearly decreases from the adhesive phase, the effective thickness of the glue joint ξ_j being approximately one tracheid long (Fig. 4c). The effective diffusion coefficient in the glue joint region D_j is then a combination of the diffusion through empty wood cells, D_w, adhesive D_a and cell wall material D_{cw}, where D_w and D_a are optimization parameters, and D_{cw} is calculated with an empirical relation following Arrhenius equation (Stamm 1959; Siau 1984):

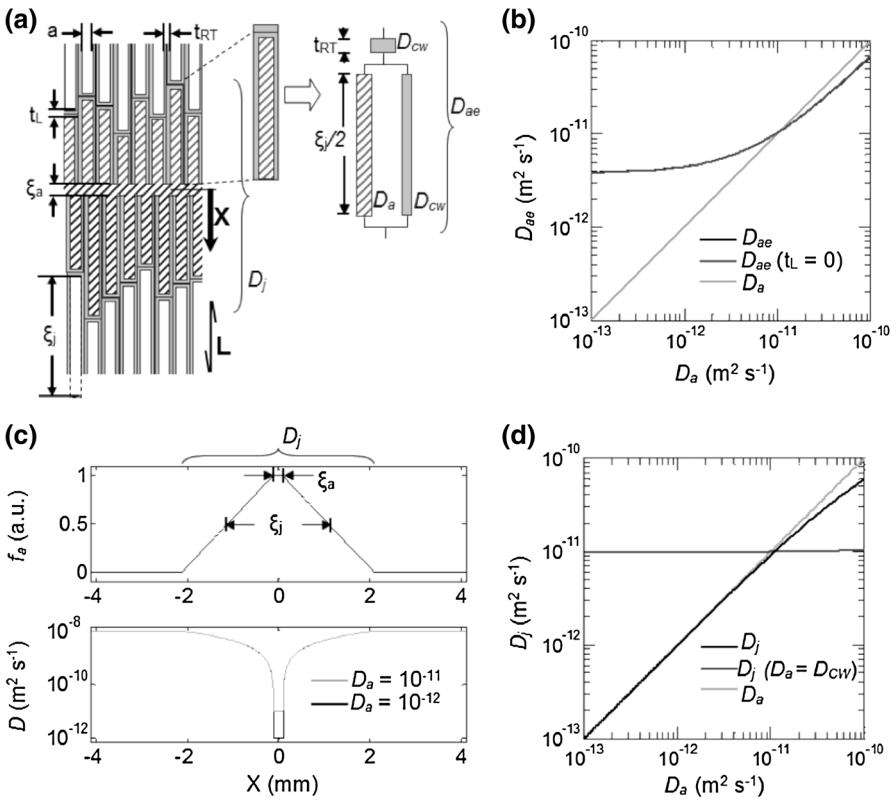

Fig. 4 Relation of macroscopic moisture diffusion with bond line microstructure. **a** Calculation model for bond line microstructure. **b** Relation between diffusion coefficients of adhesive product D_a and cell wall filled with adhesive Dae. **c** Local diffusion coefficient across the glue line D as a function of position X with respect to adhesive-filled void fraction fa. **d** Effective diffusion coefficient through glue joint D_j. The effective diffusion coefficient through a fully densified wood line ($D_a = D_{CW}$, diffusion coefficient of wood cell wall) is plotted for comparison

$$D_{\mathrm{CW}} = 2.5\times 7\times 10^{-6}\exp[-(38500-29000u)/(RT)] \tag{5}$$

with the temperature $T = 303$ K and $R = 8.31$ J mol^{-1} K^{-1} the universal gas constant. The diffusion coefficient through the glue joint is calculated by homogenization of the cellular structure represented in Fig. 4a and by repeatedly applying parallel combination of material layers sharing a same cross-section and series combination of successive layers along the diffusion direction X (Klopfer 1974; Eitelberger and Hofstetter 2011) under the approximation that stationary diffusion is instantaneously achieved within the homogenized interval:

$$\begin{aligned} D_{\mathrm{parallel}} &= f_1 D_1 + f_2 D_2 + \ldots f_{\mathrm{N}} D_{\mathrm{N}} \\ D_{\mathrm{series}}^{-1} &= f_1 D_1^{-1} + f_2 D_2^{-1} + \ldots f_{\mathrm{N}} D_{\mathrm{N}}^{-1} \end{aligned} \tag{6}$$

where D_1, D_2 … D_{N} and f_1, f_2 … f_{N} are the diffusion coefficients and material fractions for each layer, respectively. Relating macroscopic density and cell geometry with the cell porosity p:

$$p = 1-\rho_W/\rho_{\mathrm{CW}} \cong (1+2t_{\mathrm{RT}}/a)^{-1} \tag{7}$$

Where $\rho_{\mathrm{W}} = 500$ kg m^{-3} is the mean density of the samples (the dry density is used as reference value) and $\rho_{\mathrm{CW}} = 1{,}450$ kg m^{-3} is the density of the cell wall substance including microvoids (Siau 1984; Kellogg and Wangaard 1969), the diffusion coefficient through a cell full of adhesive D_{ae} is calculated as:

$$D_{\mathrm{ae}} = D_{\mathrm{a}}\left\{[(1-\rho_{\mathrm{W}}/\rho_{\mathrm{CW}})+(D_{\mathrm{CW}}/D_{\mathrm{a}})\rho_{\mathrm{W}}/\rho_{\mathrm{CW}}]^{-1}\left(1+t_{:\mathrm{L}}/\xi_{\mathrm{j}}\right)^{-1}+(D_{\mathrm{a}}/D_{\mathrm{CW}})\left(1+\xi_{\mathrm{j}}/t_{\mathrm{L}}\right)^{-1}\right\}^{-1} \tag{8}$$

and the local diffusion coefficient $D(x)$ in the interphase as a function of the fraction of adhesive-filled voids as:

$$D = f_{\mathrm{a}} D_{\mathrm{ae}} + (1-f_{\mathrm{a}}) D_{\mathrm{w}} \tag{9}$$

from which the effective diffusion coefficient through the glue joint normalized to the adhesive phase interphase thickness ξ_{a} writes:

$$D_j = \left\{\left[\int_x D(x)^{-1}dx\right]^{-1}\frac{\xi_j-\xi_a}{\xi_j}+D_a^{-1}\frac{\xi_a}{\xi_j}\right\}^{-1}\frac{\xi_a}{\xi_j} \tag{10}$$

Microscopic analyses

The glue line microstructure was thoroughly analysed after neutron investigations with light and scanning electron microscopy (Fig. 5). After measurements, the longitudinal-tangential (LT) sample surfaces were prepared with a microtome and visualized with stereomicroscopy (SZX9) with 25× magnification. A high-intensity hand-held UV lamp (UVAHAND 250 GS) was used to reveal adhesive traces in the wood cell lumina. Subsequently, the joint microstructure was studied by means of a

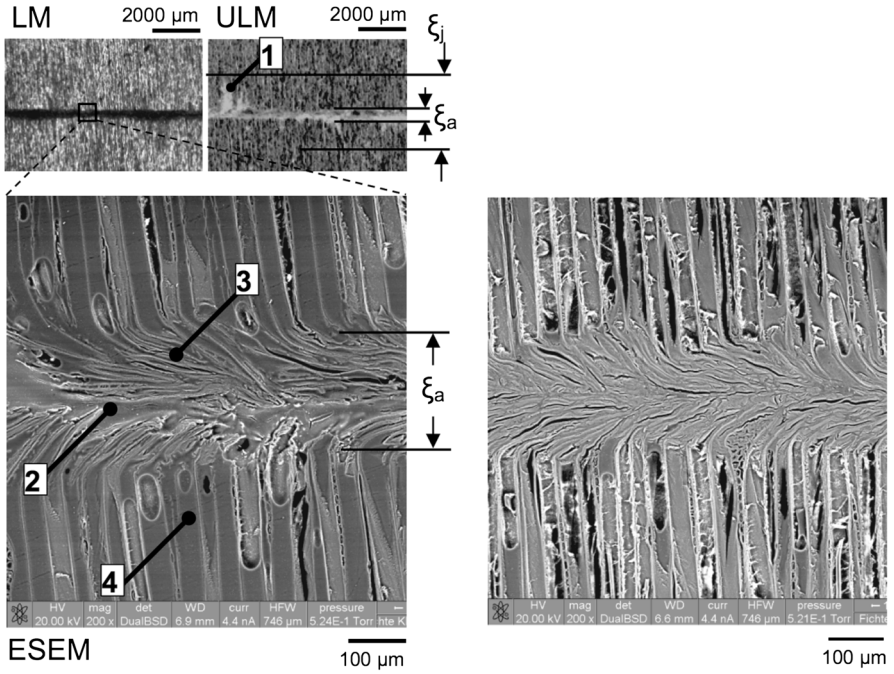

Fig. 5 Microscopic investigation of glue joint microstructure. *Top-left* light microscopy. *Top-right* light microscopy with adhesive traces (1) revealed with UV light. *Bottom* ESEM microscopy, (2) adhesive glue joints (*left* bone glue; *right* 1C-PUR), deformed (3) and undeformed (4) wood tracheids are observed

Dual Beam Scanning Electron Microscope (Quanta 200 3D) in low vacuum mode with 200x magnification.

Results and discussion

Sorption isotherms and hysteresis

The glutin-based wood adhesives show similar sorption isotherms (Fig. 6). Curves are slightly S-shaped at moderate level, up to a relative humidity about 70 %. The glutin-based adhesives did absorb up to 15 % of moisture up to this relative humidity level. Beyond 70 % RH strong water vapour absorption was recognized, reaching a 60 % weight gain at 98 % RH. In comparison, the 1-component polyurethane adhesive ran rather low at 3.5 % weight gain. The glutin-based adhesives displayed overall sigmoidal curvatures. It is known that protein-based materials sorb considerable quantities of water under standard climatic conditions, and that the extent of sorption has a sigmoidal function (Labuza 1984; Gontard et al. 1993; Cho and Rhee 2002). Because of the physical and chemical properties of most protein-based adhesives, the interactions with water vapour are complex, extensive and also fairly strong (Shamblin et al. 1998). Unlike regular repeating units in a

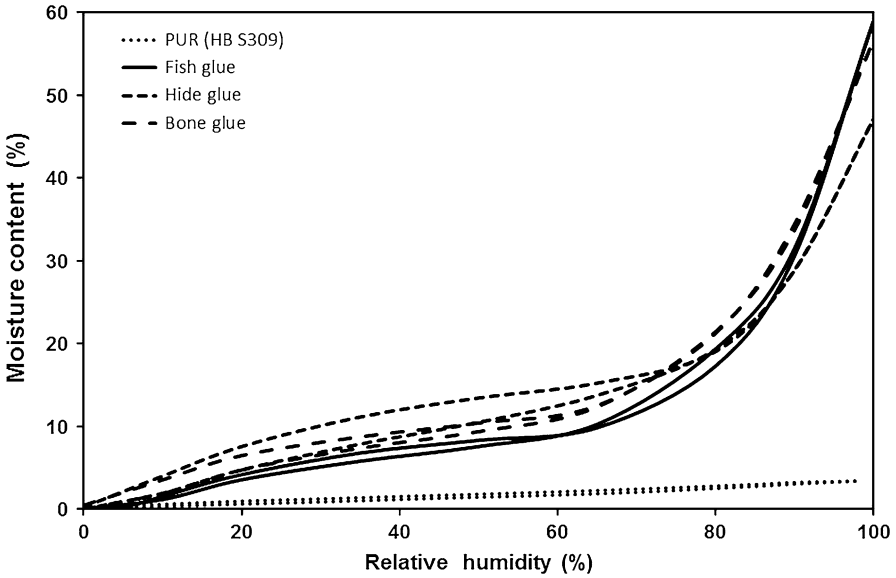

Fig. 6 Sorption isotherms of the studied adhesives tested on adhesive films

homopolymer, the many different types of assembled amorphous amino acids as well as OH- and carboxy groups give rise to a complex of molecular structures, such as loops, chains, turns and foldings. At higher relative humidity levels, these molecular structures obviously open up and vapour is able to migrate extensively within the adhesive molecular network (Norland 2006). The sorbed water increases the overall free volume of the amorphous protein material and consequently promotes molecular mobility.

Diffusion behaviour

Comparison of the mean moisture content values over the samples after 43 h diffusion (8.8–9.1 %) showed deviations of 0.2 % between neutron and gravimetric measurements. The maximum deformation occurred in cross-grain direction, with maximum strain values between 1 and 2 % for the highest measured u values (11.6 %), in qualitative agreement with literature data. Neglecting the sample deformation in Eq. 3 leads to u errors of 0.5–1.3 %, which cannot be neglected considering the small moisture variation range in Fig. 3 (6…12 %). The errors increase linearly with the sample deformation. The deformation along the grain direction is one order of magnitude lower than in cross-grain direction and thus negligible in Eq. 3.

As shown in Fig. 3, the moisture distribution in the glued samples changes in the diffusion direction X in course of the experiment ending in practically steady conditions at the end of the measurements ($t = 66$ h). The moisture distribution with respect to the sample width Y is approximately symmetric; thus, a one-dimensional diffusion model is a valid approximation. By considering only the

centre region of the sample with Y to compute the mean moisture profile along X spurious moisture transport occurring partially on the edges of the sample is filtered out.

The mean moisture profile along X as a function of time is shown in Fig. 3b. The moisture content in the moist region reaches 50 % of its final value after approximately 1 h; after 12 h, the variations are below the error level (<0.2 %). The experimental time is significantly reduced to 1 % of the time needed for measurements perpendicular to the fibre (Sonderegger et al. 2010). For an adequate optimization of the diffusion coefficients, the time snapshots need to be sampled with a uniform moisture variation rate, accordingly in this case neutron radiographies were acquired in 5 min steps until 1.6 h, afterwards in 60 min steps.

Figure 7 shows average moisture profiles along X in specific time intervals for the specific adhesive types in comparison with the moisture profiles fitted with Eq. 4. In course of the experiment, the moisture in the lamella in contact with the moist interface x_m increases and the moisture in the lamella in contact with the dry interface x_d decreases from the baseline of $u_0 = 8$ %. Due to the lower diffusion coefficient in the adhesive glue line with respect to that of wood, a barrier effect is

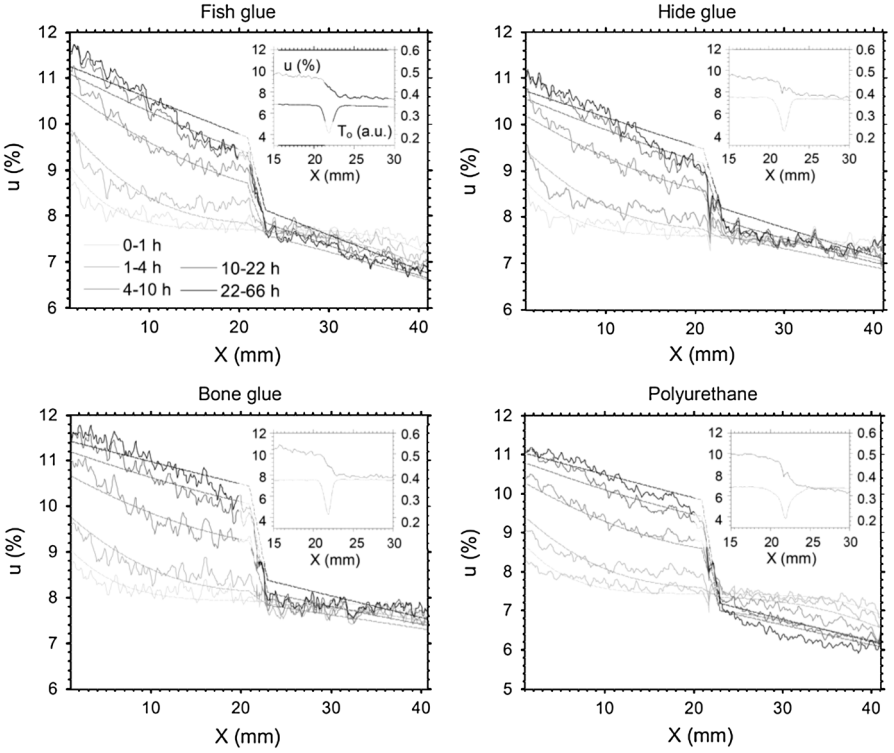

Fig. 7 Average moisture content profiles u along the diffusion direction X within specific time intervals and for each adhesive type. Experimental data (*solid lines*) is compared with simulated results with Eq. 5 for the optimized parameter set (*dashed lines*). The inlets show a detail of the measured moisture profile (*solid line*) and neutron transmission (*dotted line*) within the *glue line*

observed at the glue line, with a moisture jump of 2–3 %. The fitted moisture profiles calculated with Fick's 2nd law (Eq. 4) show a good agreement with the experimentally determined moisture profiles. More complex models, which separately differentiate the bound water in the cell wall and water vapour in the lumina are discussed in Eitelberger et al. (2011), Hozjan and Svensson (2011) and Frandsen et al. (2007). The detailed moisture profile in the glue line region is successfully resolved with the deformation correction procedure described in Fig. 2 down to the lateral resolution of the neutron measurement ($\sim$700 µm). Peak artefacts as observed in Sonderegger et al. (2010) are not present. As expected from Eq. 6, moisture decreases linearly within the glue line in steady conditions.

Table 2 shows results for the optimization of the diffusion coefficients according to the multi-step optimization described in "Determination of the wood moisture by means of neutron imaging". The optimization error e_u decreased homogeneously between steps I and III from 0.4 to 0.2 %. The optimization step IV (α_w and α_a) brought a negligible improvement (<0.001 %) to the error function as a consequence of the relatively small moisture variation range (<5 %). Consequently, moisture-independent moisture coefficients were used. In comparison, the moisture-dependent diffusion coefficients measured for polyurethane adhesive by Sonderegger et al. (2010) show also a small variation range ($0.22–0.27 \times 10^{-11}$) in the calculated moisture range.

The calculated diffusion coefficients for spruce wood ($0.9–1.3 \times 10^{-8}$) in Table 3 were in good agreement with the ones measured by Mannes et al. (2009a) ($0.9–1 \times 10^{-8}$). This provides confidence in the measurement method and the assumptions applied in the data evaluation. Moreover, the fitted surface emission coefficients and boundaries equilibrium moisture content values were in good agreement among the samples. However, the diffusion coefficients in the adhesive region for polyurethane were one order of magnitude larger than the ones observed by Sonderegger et al. (2010), the variations between specific adhesive products were not large ($3.3–8.0 \times 10^{-11}$). By trend, the glutin-based adhesives showed larger diffusion coefficients than the reference polyurethane adhesive, yet the significant variations observed between the sorption behaviour of glutin-based and polyurethane adhesives are not reflected in the neutron measurements. A possible explanation for this disagreement was found in the microstructure of the glue lines

Table 2 Diffusion coefficient optimization results for each adhesive type

Material/diffusion direction	u_m^∞ (%)	u_d^∞ (%)	$\sigma_m = -\sigma_d$ (m s^{-1})	D_w (m^2 s^{-1})	D_j (m^2 s^{-1})	e_u (%)
Fish glue/L	12.0	6.1	1.01×10^{-6}	0.9×10^{-8}	7.3×10^{-11}	0.23
Hide glue/L	11.4	6.4	0.97×10^{-6}	1.1×10^{-8}	8.0×10^{-11}	0.20
Bone glue/L	12.2	6.9	0.93×10^{-6}	1.3×10^{-8}	4.7×10^{-11}	0.21
1C PUR/L	11.8	5.5	0.82×10^{-6}	1.0×10^{-8}	3.3×10^{-11}	0.21

The results are compared with literature values for solid wood, polyurethane and cell wall at specific moisture levels. L is the grain direction, RT the cross-grain direction. The diffusion coefficients in the glue joint D_j are scaled with respect to the thickness of the adhesive phase $\xi_a = 150$ µm

Table 3 Overview of diffusion coefficients found in literature

Material/(diffusion direction)	Source	D ($u = 6$ %)	D ($u = 8$ %)	D ($u = 10$ %)	D ($u = 12$ %)
Norway spruce (L)	Mannes (2009)	0.9×10^{-8}	0.9×10^{-8}	1.0×10^{-8}	1.0×10^{-8}
PUR in Norway spruce (RT)	Sonderegger et al. (2010)	0.22×10^{-11}	0.23×10^{-11}	0.25×10^{-11}	0.27×10^{-11}
Cell wall	Siau (1984)	0.79×10^{-11}	1.00×10^{-11}	1.3×10^{-11}	1.6×10^{-11}

of the investigated samples. On the one hand, the higher penetration of the adhesive into the wood lumina leads to an adhesive interphase of vanishing thickness (Hass et al. 2012). On the other hand, the microscopic investigations, discussed in the following paragraph, revealed massive deformation and buckling in the vicinity of the glue line. These two facts indicate that the results reflect mostly the properties of the deformed wood resulting in diffusion perpendicular to the fibre direction. The adhesive only plays a minor role in the presented example. Consequently, although the measurement of diffusion properties with the presented method is able to provide physically significant diffusion values, the sample preparation needs still to be improved in order to isolate the adhesive moisture diffusion properties. As discussed next, the glue line microstructure obtained with the present sample preparation procedure is representative of adhesive bonds in the fibre direction found in timber constructions. Therefore, the calculated diffusion properties are of practical relevance. A link between the observed glue line microstructure and the measured glue line diffusion properties is established in the next section by directly applying the theoretical model of "Modelling of macroscopic moisture diffusion through bond line microstructure" to the microscopic observations. The measured diffusion coefficient values were found to be in good agreement with the theoretical predictions, further confirming the physical relevance of the measured diffusion properties.

Structural changes at the interface caused by the joining process

The light microscopy images reveal an adhesive phase of homogeneous thickness $\xi_a = 150$ μm; the adhesive penetration occurring in an average depth $\xi_j = 2.1$ mm shows good agreement with the joint thickness estimated from the neutron transmission profiles (Fig. 5). The study of the glue lines using scanning electron microscopy showed that within the adhesive layer, apart from regions with pure adhesive (2), the tracheids in the vicinity of the interface are partially buckled and deformed (Fig. 5); the wood in this zone is at least in part compressed. This phenomenon is attributed to the cutting and pressing of the timber lamellas in the fibre direction during sample preparation. The high surface roughness induces high local stresses entailing large deformation and buckling at the interface visible with high magnification in the electron microscope. The lumina of the tracheids appear to be partially filled with adhesive. This can have an additional impact on the glutin-based adhesives, which feature high water contents (50–55 %); the water penetrates the cell wall, thus reduces the strength and increases the plasticity. Such

deformation at the interface is known for other adhesive joints in or close to the grain direction, such as butt joints, finger joints and scarf joints. Figure 5 shows extreme examples of two adhesive joints (hide glue, polyurethane).

The evaluated diffusion coefficients D_j in the adhesive joint were interpreted in terms of the model described in "Modelling of macroscopic moisture diffusion through bond line microstructure". The effective diffusion coefficient D_{ae} of adhesive-filled wood cells is plotted in Fig. 4b for a range of diffusion coefficients of the adhesive product D_a. For $D_a < 10^{-11}$, a flattening of the plot is observed for D_{ae}, since moisture transport occurs through the lateral cell walls, which are the path of least resistance, the adhesive-filled lumens merely acting as a barrier to moisture diffusion. Due to the large cell aspect ratio of tracheid cells (Norway spruce, $a = 30$ µm (Wagenführ and Schreiber 1974), $\xi_j = 2.1$ mm), the effect of the end cell wall in D_{ae} can be neglected ($t_L = 0$) with a D_{ae} deviation <1 %. Figure 4c shows the local diffusion coefficient D along the interphase. In the wood phase, D is equivalent to D_w. In the adhesive interphase, the moisture transport occurs with least resistance through the fraction of wood cells not filled with adhesive, with D slowly decreasing until the vicinity of the adhesive phase D_a. Therefore, the adhesive only acts as an effective barrier to the moisture diffusion in the pure bond line. Figure 4d compares the diffusion coefficient of the joint D_j as a function of D_a. For $D_a < 10^{-11}$–10^{-13}, the deviations between D_j and D_a are small (<10 % at $D_a = 10^{-11}$, <1 % at $D_a = 10^{-12}$). Consequently, the influence of the interphase can be in practice neglected, and D_j can be used as an estimator of the diffusion properties of the adhesive product D_a as long as an adhesive phase is present between glued timber lamellas. The high D_j values observed in Table 3 can be explained under consideration of the microscopy images of the glue line microstructure (Fig. 5). Moisture diffusion occurs then through a combination of adhesive product and the compressed interphase, the path of least resistance being again dominant. Since a minimum of the diffusion coefficient through compressed wood is D_{CW}, when no lumen voids are present, the calculated D_j is for all samples higher than D_{CW}. A comparison of ESEM images for specific samples showed qualitatively an inverse correlation between the amounts of adhesive observed in the glue joint (on average highest for the samples with polyurethane and bone glue) and the measured diffusion coefficients.

The microscopic observations are representative of standard adhesive joints in or close to grain direction, such as butt joints, finger joints and scarf joints. In such joints, densification and cell damage can be induced by excessive pressure load or by local peak loads as consequence of high surface roughness (Bustos et al. 2011). Under consideration of the presented results, such adhesive joints introduce a diffusion barrier with respect to the considerably larger diffusion coefficient in wood, which is affected not exclusively by the adhesive product used but also by the wood cell deformation during specimen preparation. An effective pure adhesive phase is generally not present, which leads to reduced bonding strength properties for such joints in comparison with cross-grain bonding. If the described method is to be applied to the characterization of diffusion coefficients of the adhesive phase, the sample preparation procedure should be modified in terms of reduced pressure load, more thorough surface preparation (planing), utilization of thicker glue lines and

spacers to allow for a reproducible separation of the phases. The measured diffusion coefficients across the densified glue lines were in good quantitative agreement with theoretical predictions. Moreover, the measured diffusion coefficients and surface emission coefficients in wood phases agree well with previous investigations. This confirms the feasibility of the presented method for the characterization of moisture transport across glue joints. The presented method can also be potentially applied to the quality control of glued joints in fibre direction; the effective diffusion properties calculated across the glue lines for stitch probes can be used as input values for modelling.

Conclusion

Sorption measurements on film samples revealed strong differences between glutin-based and synthetic adhesives, with the moisture content absorbed by the glutin-based adhesives being an order of magnitude larger than the reference polyurethane adhesive. Between specific glutin-based adhesives, the differences found were not significant.

For the neutron imaging study, a modified approach was chosen as the diffusion through the glued sample was studied parallel to the fibre direction. This considerably reduces the duration of the experiments in comparison with investigations perpendicular to the fibre from several weeks or months to only about 12 h. Neutron imaging allows allocating and quantifying the moisture in the sample at any measuring time. In contrast to previous investigations, here it was possible to compensate for changes in the sample geometry due to swelling/shrinkage of wood. This allowed to correctly assess data of the whole specimen including the edge regions as well as the glue line itself. The utilization of multi-step fitting allowed optimizing the quantitative evaluation procedure with respect to the nonzero initial moisture content. Furthermore, a theoretical model was developed, which takes into account the glue line microstructure. Here, the moisture diffusion through the pure adhesive phase dominates, suggesting the potential to estimate adhesive properties from such measurements, as long as an adhesive phase layer is present between the two adherents.

The diffusion coefficients and surface emission coefficients of the wood phases were consistent with previous investigations. No significant differences between the glutin-based adhesives and the polyurethane could be determined in the current neutron imaging investigation, although polyurethane shows by trend the lowest diffusion coefficient. This can partially be attributed to the extensive penetration of the adhesive into the cell lumina, which is notably higher for bonding in fibre direction (Follrich et al. 2009). Besides this phenomenon, the small differences can be ascribed to a considerable deformation, which was observed microscopically in the vicinity of the joint. The wood cells in the vicinity of the adhesive line show to a great extent buckling and densification; thus, the moisture transport occurs in this region through the cell wall perpendicular to the fibre direction. Under consideration of the densification, the modelled diffusion coefficients across the glue line were in agreement with the measured values.

Although information on the pressure applied during the sample preparation is not available, the results can still be regarded as representative of real glue joint in fibre directions such as butt joints or finger joints. It has to be stated that throughout the bonding zone, the adhesive did not form a closed film, which leads to a diffusion behaviour comparable to that of solid wood panels with grooved middle layer.

To allow characterization of the diffusion properties of the adhesive phase, a modification of the sample preparation procedure is required to avoid the phenomenon of densification and deformation in the region of the adhesive joint. A possible solution would, for example, be to introduce intermediate foils between the two glued lamellas to guarantee a minimum thickness of the adhesive phase. Furthermore, additional diffusion experiments perpendicular to the fibre should be performed to quantitatively validate the calculated adhesive diffusion coefficient.

Acknowledgments The authors kindly acknowledge the Purbond AG and Kremer AG for the supply of adhesives, Mr. J.-A. Schmidt for sample preparation and supporting the experiments. The support of Mrs. G. Peschke with ESEM is gratefully acknowledged.

References

Blau B, Clausen KN, Gvasaliya S et al (2009) The swiss spallation neutron source SINQ at the Paul Scherrer Institut. Neutron News 20(3):5–8

Bustos C, Hernandez RE, Beauregard R, Mohammad M (2011) Effects of end-pressure on the finger-joint quality of black spruce lumber: a microscopic analysis. Maderas. Ciencia y tecnología 13(3):319–328

Cho SY, Rhee C (2002) Sorption characteristics of soy protein films and their relation to mechanical properties. Lebensm Wiss Technol 35:151–157

DIN ISO 12572:2001. Hygrothermal performance of building materials and products: Determination of water vapour transmission properties (ISO 12572:2001); German version EN ISO 12572:2001

Eitelberger J, Hofstetter K (2011) Prediction of transport properties of wood below the fiber saturation point: A multiscale homogenization approach and its experimental validation. Part II: steady state moisture diffusion coefficient. Compos Sci Technol 7:145–151

Eitelberger J, Svensson S (2012) The sorption behavior of wood studied by means of an improved cup method. Transp Porous Med 92:321–335

Eitelberger J, Svensson S, Hofstetter K (2011) Theory of transport processes in wood below the fiber saturation point. Physical background on the microscale and its macroscopic description. Holzforschung 65:337–342

Follrich J, Frybort S, Teischinger A, Muller U (2009) Fillets formed by adhesive bonding of axially oriented webs to flat grain wood pieces and their effects on bond strength. J Sandwich Struct Mater 11:245–256

Frandsen HL, Damkilde L, Svenson S (2007) A revised multi-Fickian moisture transport model to describe non-Fickian effects in wood. Holzforschung 61:563–572

Gereke T, Anheuser K, Lehmann E, Kránitz K, Niemz P (2011) Moisture behaviour of recent and naturally aged wood. Wood Res 56:33–42

Gontard N, Guilbert S, Cuq J (1993) Water and glycerol as plasticizer affect mechanical and water vapor barrier properties of an edible wheat gluten film. J Food Sci 58:206–211

Hass P, Wittel F, Mendoza M, Herrmann HJ, Niemz P (2012) Adhesive penetration in beech wood: experiments. Wood Sci Technol 46:243–256

Hassanein RK (2006) Correction methods for the quantitative evaluation of thermal neutron tomography. Dissertation, ETH Zurich, Switzerland

Hozjan T, Svensson S (2011) Theoretical analysis of moisture transport in wood as an open porous hygroscopic material. Holzforschung 65:97–102

Kellogg RM, Wangaard FF (1969) Variation in the cell-wall density of wood. Wood Fiber 1:180–204

Klopfer H (1974) Wassertransport durch diffusion in feststoffen. Bauverlag GmbH, Wiesbaden and Berlin

Kollmann (1965) Einfluss der Vorbehandlung insbesondere Wärmevorbehandlung von Holz und Holzwerkstoffen vor der Verleimung auf die Leimbindefestigkeit. Westdeutscher Verlag, Cologne

Labuza, TP (1984) Determination of moisture sorption isotherms. In: Moisture Sorption: Practical Aspects of Isotherm Measurement and Use. St. Paul, MN: American Association of Cereal Chemists: 64–73

Lanvermann C, Sanabria S, Mannes D, Niemz P (2013) Combination of neutron imaging (NI) and digital image correlation (DIC) to determine intra-ring moisture variation in Norway spruce. Holzforschung. doi:10.1515/hf-2012-0171

Lehmann EH, Vontobel P, Wiezel L (2001) Properties of the radiography facility NEUTRA at SINQ and its potential for use as European reference facility. Nondestruct Test Eval 16:191–202

Mannes D (2009) Non-destructive testing of wood by means of neutron imaging in comparison with similar methods. Dissertation, ETH Zurich, Switzerland

Mannes D, Sonderegger W, Hering S, Lehmann E, Niemz P (2009a) Non-destructive determination and quantification of diffusion processes in wood by means of neutron imaging. Holzforschung 63:589–596

Mannes D, Josic L, Lehmann E, Niemz P (2009b) Neutron attenuation coefficients for non-invasive quantification of wood properties. Holzforschung 63(5):472–478

Mannes D, Schmidt JA, Niemz P, Volkmer T (2012) Investigations on the influence of the adhesive type on the capillary water transport in wood parallel to the fibre direction. Bauphysik 34(2):61–65

Norland RE (2006) Fish gelatin and fish flue. In: Tracton AA (ed) Coatings technology handbook, 3rd edn. CRC Press, Boca Raton, pp 65-1–65-4

Shamblin SL, Hancock BC, Zografi G (1998) Water vapor sorption by peptides, proteins and their formulations. Eur J Pharm Biopharm 45:239–247

Siau JF (1984) Transport process in wood. Springer, Berlin

Sonderegger W, Hering S, Mannes D, Vontobel P, Lehmann E, Niemz P (2010) Quantitative determination of bound water diffusion in multilayer boards by means of neutron imaging. Eur J Wood Prod 68:341–350

Stamm AJ (1959) Bound-water diffusion into wood in across-the-fiber directions. Forest Prod J 10(10):524–528

Volkmer T, Schmidt JA, Kranitz K, Niemz P (2012) Untersuchungen zum Einfluss der Klebstoffart auf den Diffusionswiderstand von Holzverklebungen. Bauphysik 34(2):55–59

Wagenführ R, Scheiber C (1974) Holzatlas. VEB Fachbuchverlag, Leipzig